ICIC Express Letters
Part B: Applications
Volume **11**, Number **8**, August **2020**

 ISSN 2185-2766
pp. **781–790**

PERFORMANCE EVALUATION OF SLIDING MODE AND LINEAR QUADRATIC REGULATOR (LQR) CONTROL IN INTERLEAVED DOUBLE DUAL BOOST CONVERTER FOR ELECTRIC VEHICLE APPLICATIONS

J. S. V. Siva Kumar[1,2] and P. Mallikarjuna Rao[1]

[1]Department of Electrical Engineering
Andhra University
Visakhapatnam-530003, Andhra Pradesh, India
jsvsivakumar99@gmail.com; sivakumar.jsv@gmrit.edu.in

[2]Department of Electrical and Electronics Engineering
GMR Institute of Technology
Rajam-532127, Srikakulam Dist., Andhra Pradesh, India

Received November 2019; accepted February 2020

Abstract. *With expanded carbon emanations in condition, impacts of a worldwide temperature alteration are getting extreme. Because of this reason automobile industry people are paying more concentration on green technology – hybrid electric vehicles. Of the available green technologies, fuel cell provides higher energy density but is expensive. In perspective on this, a legitimate system must be inferred to use the energy efficiently to make the electric vehicles reasonable. Due to the low voltage output from fuel cell, boost converters are used to meet the load requirements. Interleaved Double Dual Boost (IDDB) converters are recommended to increase the efficiency of the converter and in turn to reduce overall weight of the vehicle. In this paper, both sliding mode control and LQR control technique are implemented to improve the transient response of the fuel cell powered IDDB converter for various load conditions. Moreover, the performances of both controllers are compared. The output voltages, output currents and input currents of IDDB converter with sliding mode and LQR controller are obtained and verified in the simulated environment using MATLAB/Simulink.*

Keywords: Hybrid electric vehicles, Fuel cell, IDDB converter, High voltage gain, Sliding mode controller, LQR controller

1. **Introduction.** One of the primary reasons for the introduction of electric vehicles into the market is the concern over greenhouse gas emissions and their contribution to global warming. In any case, the use of petroleum derivatives, carbon-based mixes, in the vehicles, brings about tremendous measures of ozone depleting substances. As indicated by a few examinations, a large portion of the thickly populated urban communities are confronting negative air quality. Interestingly, electric vehicles utilize electrical vitality for drive, coming about in eco-accommodating transportation [1]. Electric vehicles use battery, ultra-capacitor, Fuel Cell (FC) as energy source for propulsion system. Of these, fuel cell, because of high power density and green source of electrical energy, was demonstrated to be a superior decision as an essential source of energy in EV. However, due to the slower response of FC, they cannot react quicker for unexpected changes in load and hence an ultra-capacitor is suggested for propulsion during dynamic condition. Ultra-capacitors have high energy density but low power densities, which make them charge as well as discharge at a faster rate. This nature allows the ultra-capacitor to provide the energy during transients [1].

DOI: 10.24507/icicelb.11.08.781

Typically voltage level of FC is extremely low but to run the motor requires high voltage. Hence, a step-up chopper is required to boost the voltage level of FC. It is quite a challenging task to maintain high efficiency at such voltage gain requirements [2,3]. For a given power, low input voltage results in high input current [2-6]. Such high current enforces the boost converter to operate at small duty cycle affecting the size of the inductor and output capacitor and therefore results in increased losses and reduced efficiency.

Hence, for high power applications such as EV, a high power converter is required for boosting up voltage level of FC, which can deal with high current and high voltage at the input and output side respectively without affecting the efficiency. The most efficient way to tackle this problem is by interleaving multiple conventional-boost converters.

This paper verifies the feasibility of interleaved double dual boost proposed with the objective of achieving higher voltage gain in contrast to the classical boost converter [7-9]. This topology was chosen among others having high gain properties owing to the possibility of phase interleaving that allows the modular characteristics of the converter for high power applications.

An efficient controller is required for regulating output voltage at the nominal value even under load perturbations that typically happen in electric vehicles. This paper presents a sliding mode and LQR control of an interleaved double dual boost converter [10-15] and the output voltages, currents and input currents are verified and compared in a simulation environment using MATLAB/Simulink.

2. **Modeling of the *N*-Phase IDDB Converter.** The IDDB with two phases is shown in Figure 1, where 'R_o' represents the load. Each phase of the converter has a conventional boost module with an inductor and its corresponding pair of switches. Phase1 and capacitor C_1 are denoted by "module 1" while Phase2 and capacitor C_2 are denoted by "module 2" and both the modules are assumed to be symmetric.

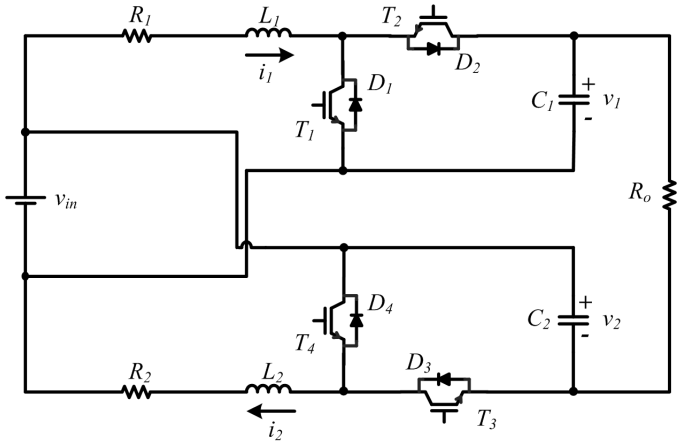

FIGURE 1. IDDB with two phases

The variable δ is the duty cycle and it is identical to both the modules. The model is concerned with the capacitors voltages that have an indirect relationship with output voltage. However, it is noteworthy that the output voltage depends on the input voltage. This infers that any change in input voltage reflects in the output voltage and can be compensated by regulating output-capacitor voltage references. Any attempt to directly control the output voltage, ignoring module voltages, would result in an imbalance of these voltages, resulting in distorted symmetry in the wave shape.

As pointed, this topology facilitates modular structure permitting more than two phases. In order to attain symmetry, an even multiple of phases are preferred. This section is to generalize the converter modeling to N-phase topology.

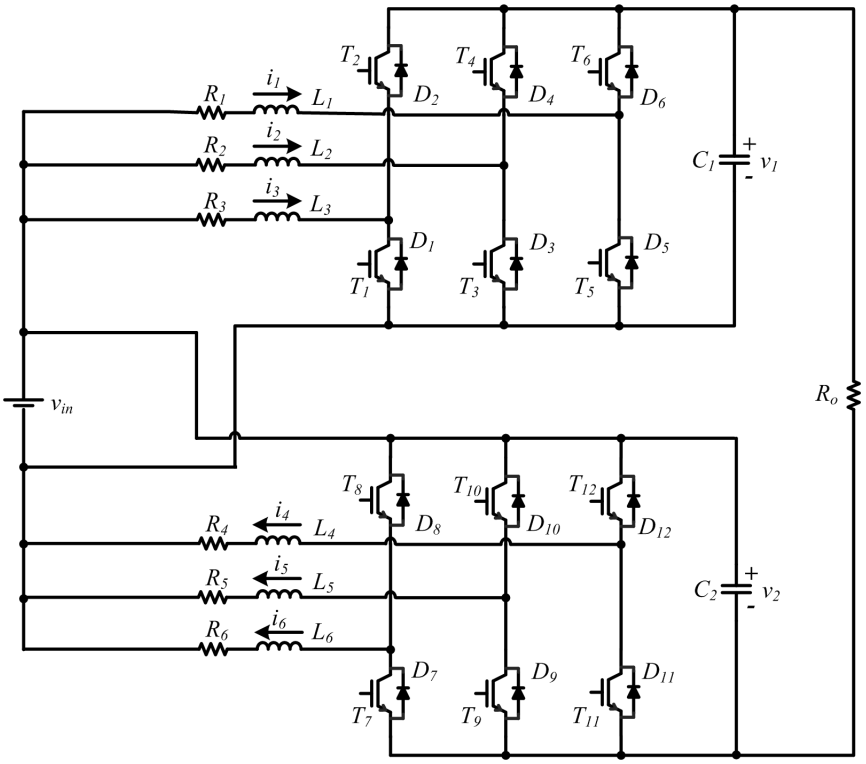

FIGURE 2. Six phase IDDB converter

The combination of the phases that are connected to the capacitor C_1 and capacitor C_2 itself forms module 1 and vice versa for module 2. As a demonstration, the six phase converter is shown in Figure 2 to depict multiple phases.

The source current is given by

$$i_{in} = i_1 + i_2 + i_3 + \cdots + i_N - i_0 \tag{1}$$

The N-phase IDDB has $N + 2$ state variables, here chosen as the representing 'N' inductor currents and two capacitor voltages.

The differential equation for the current in each of the $N/2$ inductors of module 1 is given by

$$\frac{d}{dt}I_k = \frac{1}{L_k}\left(-R_k I_k - V_1\bar{\delta}_k + V_{in}\right) \tag{2}$$

for $k = 1, 2, 3, \ldots, N/2$. It is similar for $k = (N/2) + 1$ to N.

The differential equation for the voltage in C_1 is given by V_1

$$\frac{d}{dt}V_1 = \frac{1}{C_1}\left[\left(\sum_{k=1}^{\frac{N}{2}} I_k\bar{\delta}\right) + \frac{-V_1 - V_2 + V_{in}}{R_0}\right] \tag{3}$$

Similar expression will be obtained for the voltage across C_2.

By exploring the symmetry of the system mentioned above (Figure 1), it can be generalized for N-phase system, then $I_1 = I_2 = \cdots = I_N = I$ and $\delta_1 = \delta_2 = \cdots = \delta_N = \delta$

$$\frac{d}{dt}I = \frac{1}{L}\left(-RI - V\bar{\delta} + V_{in}\right) \tag{4}$$

$$\frac{d}{dt}V = \frac{1}{C}\left[\frac{\left(N\bar{\delta}I\right)}{2} + \frac{-2V + V_{in}}{R_0}\right] \tag{5}$$

In the state-space form, the state vector is

$$X = \begin{bmatrix} I & V \end{bmatrix}^I \tag{6}$$

While the system and input matrixes are

$$A = \begin{bmatrix} \dfrac{-R}{L} & \dfrac{-\bar{\delta}}{L} \\ \dfrac{N\bar{\delta}}{2C} & \dfrac{-2}{R_0C} \end{bmatrix}, \qquad B = \begin{bmatrix} \dfrac{1}{L} \\ \dfrac{1}{R_0C} \end{bmatrix} \tag{7}$$

The set of attainable equilibrium points of the converter is given by

$$X_{eq} = -A^{-1}BU \tag{8}$$

where $U = [v_{in}]$ and from above, the set of equilibrium points can be written as

$$X_{eq} = \begin{bmatrix} I_{eq} \\ V_{eq} \end{bmatrix} = \begin{bmatrix} \dfrac{2+2\delta}{4R + NR_0(1-\delta)^2} \\ \dfrac{2R + NR_0(1-\delta)}{4R + NR_0(1-\delta)^2} \end{bmatrix} \tag{9}$$

Using the state-space averaging method, and assuming the small-signal approximation, the equivalent linear system near the equilibrium point is given by

$$\dot{\tilde{x}} = A\tilde{x} + [(A_1 - A_2)X + (B_1 - B_2)U]\tilde{\delta} \tag{10}$$

where A_1 and A_2 are the matrices when δ value for 1 and 0 respectively, X is equilibrium point and using above values the equation can be simplified into

$$\dot{\tilde{x}} = A\tilde{x} + [(A_1 - A_2)X]\tilde{\delta} \tag{11}$$

Substituting all the above values finally

$$\dot{\tilde{x}} = \begin{bmatrix} \dot{\tilde{i}} \\ \dot{\tilde{v}} \end{bmatrix} = \begin{bmatrix} \dfrac{-R}{L}\tilde{i} - \dfrac{\bar{\delta}}{L}\tilde{v} + \dfrac{V_{in}}{L}\left\{\dfrac{2R + NR_0(1-\delta)}{4R + NR_0(1-\delta)^2}\right\}\tilde{\delta} \\ \dfrac{N\bar{\delta}}{2C}\tilde{i} - \dfrac{2}{R_0C}\tilde{v} - \dfrac{NV_{in}}{2C}\left\{\dfrac{(2+2\delta)}{4R + NR_0(1-\delta)^2}\right\}\tilde{\delta} \end{bmatrix} \tag{12}$$

3. **Sliding Mode Controller Methodology.** The reference currents of the inductors are obtained by applying small signal analysis. The feedback controller is designed to achieve good response. Due to fast and robustness requirement of the converter, a sliding mode controller is designed, which is a large signal model, resulting in global stability. A sliding surface is defined as follows.

From this $S = \tilde{v} + k\tilde{i}$ then $\dot{S} = \dot{\tilde{v}} + k\dot{\tilde{i}}$

$$\begin{aligned} \dot{S} = {} & \frac{N\bar{\delta}}{2C}\tilde{i} - \frac{2}{R_0C}\tilde{v} - \frac{NV_{in}}{2C}\left\{\frac{(2+2\delta)}{4R + NR_0(1-\delta)^2}\right\}\tilde{\delta} \\ & + k\left[\frac{-R}{L}\tilde{i} - \frac{\bar{\delta}}{L}\tilde{v} + \frac{V_{in}}{L}\left\{\frac{2R + NR_0(1-\delta)}{4R + NR_0(1-\delta)^2}\right\}\right]\tilde{\delta} \end{aligned} \tag{13}$$

Separating $\tilde{v}$, $\tilde{i}$ terms and $\tilde{\delta}$ terms then

$$\begin{aligned} \dot{S} = {} & \frac{N\bar{\delta}}{2C}\tilde{i} - \frac{2}{R_0C}\tilde{v} - k\frac{R}{L}\tilde{i} - k\frac{\bar{\delta}}{L}\tilde{v} + \left[k\frac{V_{in}}{L}\left\{\frac{2R + NR_0(1-\delta)}{4R + NR_0(1-\delta)^2}\right\}\right. \\ & \left. - \frac{NV_{in}}{2C}\left\{\frac{(2+2\delta)}{4R + NR_0(1-\delta)^2}\right\}\right]\tilde{\delta} \end{aligned} \tag{14}$$

The above equation can be represented as $\dot{S} = f(x) + u$.

Sliding mode will be there when $\dot{S} = 0$.

The generalized control structure $u = -f(x) - k_1 sign(S)$.

From the above equation controlling signal $\tilde{\delta}$ is obtained

$$\tilde{\delta} = \frac{\left[\left\{-\frac{N\bar{\delta}}{2C}\tilde{i} + \frac{2}{R_0C}\tilde{v} + k\frac{R}{L}\tilde{i} + k\frac{\bar{\delta}}{L}\tilde{v}\right\} - k_1 sign(s)\right]}{\left[k\frac{V_{in}}{L}\left\{\frac{2R+NR_0(1-\delta)}{4R+NR_0(1-\delta)^2}\right\} - \frac{NV_{in}}{2C}\left\{\frac{(2+2\delta)}{4R+NR_0(1-\delta)^2}\right\}\right]} \tag{15}$$

The control diagram of implemented controller is shown in Figure 3, where V_1 and V_2 are the module 1 and module 2 capacitor-voltages respectively. i_1, i_2, i_3, i_4, i_5 and i_6 are respectively phase currents. V_1 is the DC link voltage input to the sliding mode controller for module 1 while V_2 is for the module 2. Similarly, i_1, i_2 and i_3 are the input to sliding mode controller of module 1 and i_4, i_5 and i_6 are the input to the module 2 sliding mode controller. Duty ratio is the output of the SMC and is used to generate PWM pulses to control the power switches.

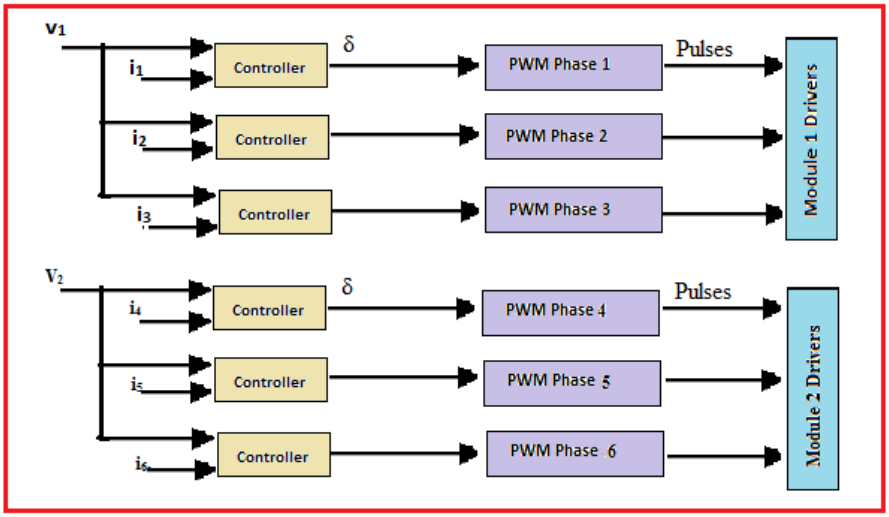

FIGURE 3. Control diagram of the implemented controllers

4. **Linear Quadratic Regulator (LQR) Controller Methodology.** The finite horizon, Linear Quadratic Regulator (LQR) is given by

$$\dot{x} = Ax + Bu, \quad y = Cx, \quad x \in \Re^n,\ u \in \Re^m,\ y \in \Re^p,\ x_0 \text{ given}$$

$$J = \frac{1}{2}\int_0^T \left(x^T Q x + u^T R u\right) dt \tag{16}$$

where A and B values are given in Equation (7), $Q \geq 0$, $R > 0$, $P \geq 0$, are symmetric, positive (semi-) definite matrices. The Q and R are weight matrices for states and control input respectively.

The LQR control input is given by

$$u = -kx \tag{17}$$

'k' is LQR gain and is given by

$$k = R^{-1}B^T P \tag{18}$$

and 'P' can be obtained from algebraic Ricatti equation solution of

$$A^T P + PA - PBR^{-1}B^T P + Q = 0 \tag{19}$$

5. **Results and Discussion.** The IDDB converter is modeled and its performance of the system by employing sliding mode and LQR controllers is verified on MATLAB/Simulink. The results of whole system parameters are shown below. In these two phases and six phase IDDB converter with sliding mode and LQR controllers simulation results are explained. The nominal parameters $V_{in} = 60\text{V}$, $R = 0.15\Omega$, $L = 535\mu\text{H}$, $C = 470\mu\text{F}$, $R_o = 59\Omega$, and $f_{sw} = 10\text{kHz}$ are considered for simulation [8].

The currents flowing through the inductor of the two phases of sliding mode and LQR controllers are presented in Figures 4 and 5. It is clearly observed that the current in each inductor has a current ripple of 8A in SM and 12A in LQR controller IDDB.

The output currents flowing through the load of the sliding mode and LQR controllers based two phase IDDB are presented in Figures 6 and 7. It is clearly observed that the output current in SM is nearly 7A whereas 5A in LQR controller IDDB. From this for the

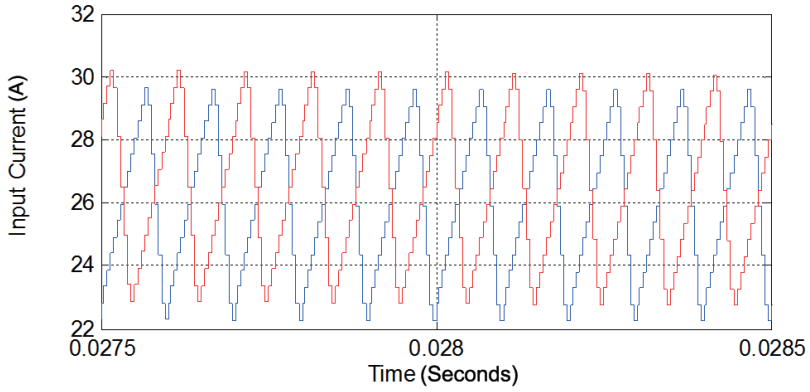

FIGURE 4. Input current to two phase IDDB in SM

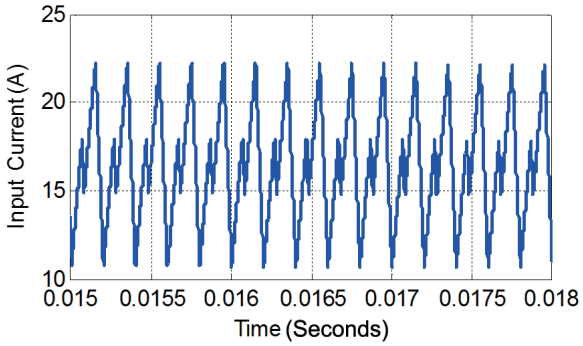

FIGURE 5. Input current to two phase IDDB in LQR

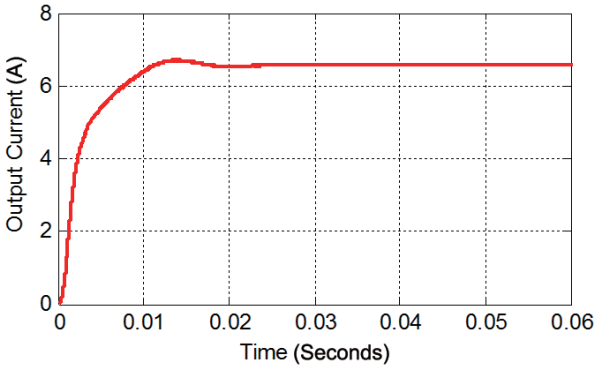

FIGURE 6. Output current to two phase IDDB in SM

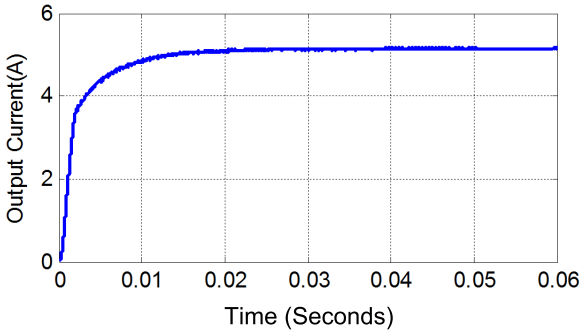

FIGURE 7. Output current to two phase IDDB in LQR

same input voltage, sliding mode controller is giving more output current as compared to LQR control of IDDB converter.

The output voltages across the load of the sliding mode and LQR controllers based two phase IDDB are presented in Figures 8 and 9. It is clearly observed that the output voltage across load in SM is nearly 400V whereas 300V in LQR controller IDDB. From this for the same input voltage, sliding mode controller is giving more output voltage as compared to LQR control of IDDB converter.

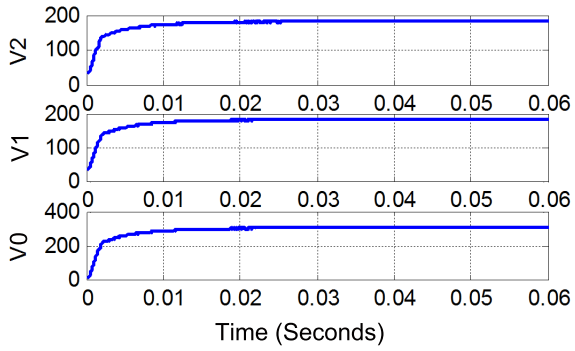

FIGURE 8. Output voltage of two phase IDDB in SM

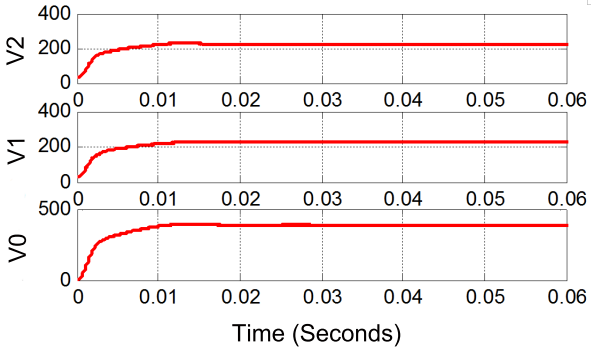

FIGURE 9. Output voltage of two phase IDDB in LQR

The currents flowing through the inductor of the six phases of sliding mode and LQR controllers are presented in Figures 10 and 11. It is clearly observed that the current in each inductor has a current ripple of 8A in SM and 12A in LQR controller IDDB. However, the magnitude of the input current through the inductor decreases with the increasing number of phases. In two phase its value is nearly 30A whereas in six phase the value is 18A only.

The output currents flowing through the load of the sliding mode and LQR controllers based six phase IDDB are presented in Figures 12 and 13. It is clearly observed that the

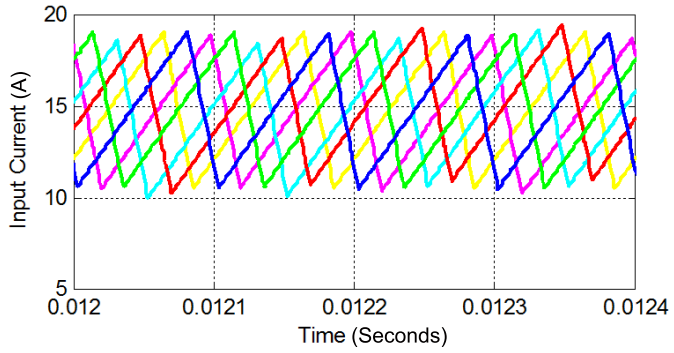

FIGURE 10. Input current to six phase IDDB in SM

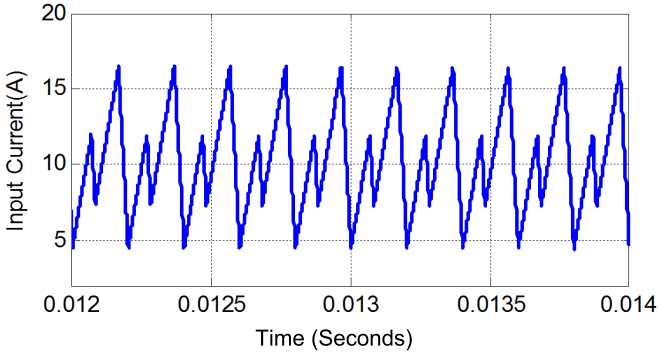

FIGURE 11. Input current to six phase IDDB in LQR

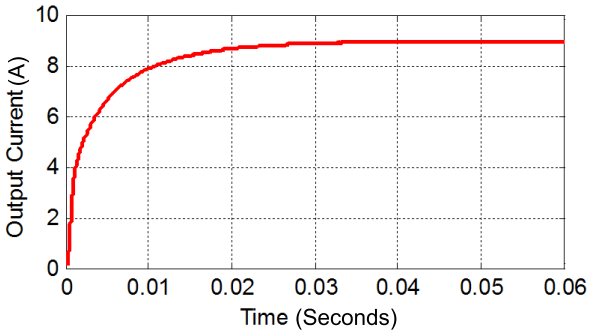

FIGURE 12. Output current to six phase IDDB in SM

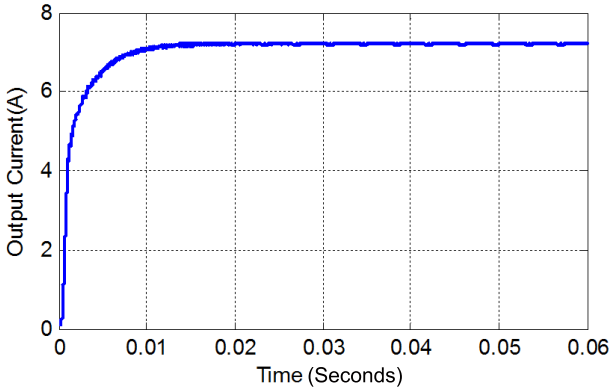

FIGURE 13. Output current to six phase IDDB in LQR

output current in load in SM is nearly 9A whereas 7A in LQR controller IDDB. From this for same input voltage, sliding mode controller is giving more output current as compared to LQR control of IDDB. In addition, these values are more as compared to two phase IDDB.

The output voltages across the load of the sliding mode and LQR controllers based six phase IDDB are presented in Figures 14 and 15. It is clearly observed that the output voltage across load in SM is nearly 500V whereas 400V in LQR controller IDDB. From this for same input voltage, sliding mode controller gives more output voltage as compared to LQR control of IDDB. In addition, these values are more as compared to two phase IDDB.

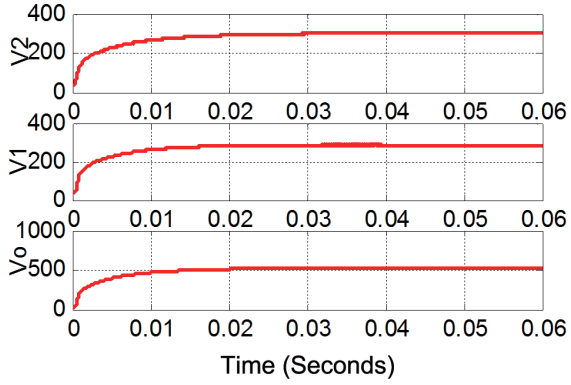

FIGURE 14. Output voltage of six phase IDDB in SM

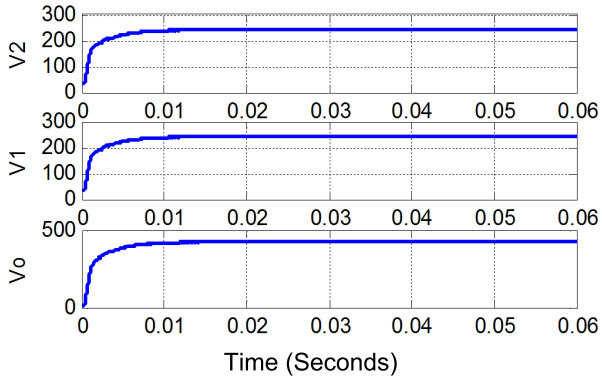

FIGURE 15. Output voltage of six phase IDDB in LQR

6. **Conclusions.** This paper has briefed the modeling and small signal analysis of the general N-phase IDDB converter. The sliding mode and LQR control design for this converter is illustrated for two phase as well as for six phase. It is evident from the results that as the number of phases increases, the power handling capability of the converter is found to be increasing. Hence, the converter can be upgraded with more number of phases as per the load requirements. The symmetry of the converter and the control action were utilized in order to reduce the complexity of the model. In addition, sliding mode controller is robust in nature as compared to LQR controller. Simulation results in MATLAB/Simulink were provided in support of the theoretical analysis. In future this DC output is connected to inverter to check the performance of electric vehicle.

REFERENCES

[1] H. El Fadil, F. Giri, S. M. Ieee, J. M. Guerrero and S. Member, Modeling and nonlinear control of FC/super capacitor hybrid energy storage system for electric vehicles, *IEEE Trans. Vehicular Technology*, vol.63, no.7, pp.3011-3018, 2014.

[2] A. Shahin, M. Hinaje, J.-P. Martin, S. Pierfederici, S. Rael and B. Davat, High voltage ratio DC-DC converter for fuel-cell applications, *IEEE Trans. Ind. Electron.*, vol.57, no.12, pp.3944-3955, 2010.
[3] L. S. Yang, T. J. Liang, H. C. Lee and J. F. Chen, Novel high step-up DC-DC converter with coupled-inductor and voltage-doubler circuits, *IEEE Trans. Ind. Electron.*, vol.58, no.9, pp.4196-4206, 2011.
[4] J. S. V. Siva Kumar and P. Mallikarjuna Rao, Design and simulation of front end converter for fuel cell based electric vehicle applications, *IEEE International Conference on Power, Control, Signals and Instrumentation Engineering (ICPCSI)*, Chennai, 2017.
[5] J. S. V. Siva Kumar and P. Mallikarjuna Rao, Design and simulation of DC-DC converter for fuel cell based electric vehicle with closed loop operation, *Springer International Conference on Soft Computing in Data Analytics (SCDA 2018)*, Andhrapradesh, 2018.
[6] J. S. V. Siva Kumar and P. V. Sateesh, Design and simulation of a current fed full bridge voltage doubler converter with high voltage gain for fuel cell based electric vehicle, *Journal of Advanced Research in Dynamical and Control Systems*, vol.9, no.16, pp.110-121, 2017.
[7] P. Thounthong, P. Sethakul and B. Davat, Modified 4-phase interleaved fuel cell converter for high-power high-voltage applications, *Proc. of IEEE Int. Conf. Ind. Technol.*, pp.1-6, 2009.
[8] F. S. Garcia, J. A. Pomilio and G. Spiazzi, Modeling and control design of the six-phase interleaved double dual boost converter, *Proc. of the 9th IEEE/IAS Int. Conf. Ind. Appl.*, pp.1-6, 2010.
[9] S. Choi, V. G. Agelidis, J. Yang, D. Coutellier and P. Marabeas, Analysis, design and experimental results of a floating-output interleaved-input boost-derived DC-DC high-gain transformer-less converter, *IET Power Electron.*, vol.4, no.1, pp.168-180, 2011.
[10] J. Yang, S. Li and X. Yu, Sliding-mode control for systems with mismatched uncertainties via a disturbance observer, *IEEE Trans. Ind. Electron.*, vol.60, no.1, pp.160-164, 2013.
[11] A. Kanchanaharuthai and E. Mujjalinvimut, An improved backstepping sliding mode control for power systems with superconducting magnetic energy storage system, *International Journal of Innovative Computing, Information and Control*, vol.15, no.3, pp.891-904, 2019.
[12] H. A. Bouziane, R. B. Bouiadjra and M. B. Debbat, Design of robust LQR control for DC-DC multilevel boost converter, *The 4th International Conference on Electrical Engineering (ICEE)*, 2015.
[13] C. Li, G. Wang, Y. Fan and Y. Li, An integral and time-varying sliding mode speed control of switched reluctance motor drives, *ICIC Express Letters, Part B: Applications*, vol.8, no.3, pp.601-608, 2017.
[14] Y. Han, L. Liu and Y. Fang, Adaptive robust control for the speed system of cold strip main rolling mill based on global integral sliding mode, *ICIC Express Letters, Part B: Applications*, vol.8, no.3, pp.593-600, 2017.
[15] G. Xia, J. Xue, C. Sun and Y. Yang, Sliding mode control with RBFNN compensation for dynamic positioning of ship with disturbances and input saturation, *International Journal of Innovative Computing, Information and Control*, vol.14, no.6, pp.2163-2174, 2018.